Linear variable filters fabricated by ion beam etching with triangle-shaped mask and normal film coating technique

Bin Sheng (盛 斌), Peng Chen (陈 鹏)*, Chunxian Tao (陶春先), Ruijin Hong (洪瑞金), Yuanshen Huang (黄元申), and Dawei Zhang (张大伟)

Engineering Research Center of Optical Instruments and Systems, Ministry of Education and Shanghai Key Laboratory of Modern Optical Systems, University of Shanghai for Science and Technology, Shanghai 200093, China

**Corresponding author: qjzxchp123@126.com*

Received June 14, 2015; accepted October 16, 2015; posted online November 6, 2015

In this Letter, we propose a method of fabricating linear variable filters by ion beam etching with masking mechanisms. A triangle-shaped mask is designed and set between the ion source and sample. During the ion etching, the sample is moved back and forth repeatedly with a constant velocity for the purpose of obtaining the linearly varied thickness of the cavity. Combined with ion beam assistant thermal oxidative electron beam evaporation deposition technology, we finish the fabrication of linear variable filters, whose filtering range is from 500 to 580 nm. The measured results indicate that the transmittance and bandwidth at the peak wavelength are around 40% and 3 nm.

OCIS codes: 230.7408, 220.4610, 310.4165.

doi: 10.3788/COL201513.122301.

A linear variable optical filter (LVOF) is an optical interference filter whose spectral functionality varies along one direction of the filter. Compared to optical splitting elements such as prisms and gratings, LVOFs are widely proposed for their advantages of miniaturization, multiple filtering bands, and tunable filtering wavelengths. They also can be utilized to make up a spectrum detector with a CCD/CMOS camera, remarkably improving the simplicity, stability, and efficiency of the optical splitting system[1–3]. A LVOF set as the pivotal optical splitting component of a spectrometer can be applied to applications in aerospace, field detection, atmospheric monitoring, biological fluid detection, chemical sensors, spectral imaging, and so on[4–6]. As such, relevant research on LVOF has attracted extensive interest[7–15].

The methods of fabricating LVOFs have been widely investigated. Abel-Tibérini *et al.* proposed a method for manufacturing linear variable filters based on the use of correcting masks that combine both the rotation and translation movements of the masks and substrates[11]. Piegari and Bulir used a similar method by introducing proper masks into the deposition system, and exposing the substrate to the flux of particles at different time intervals in different zones[12,13]. Emadi *et al.* reported the integrated circuit-compatible fabrication of vertically tapered cavity layers in LVOF by using resist reflow[14]. Most researchers put their focus on forming tapered cavity layers during deposition; however, less attention is paid to applying mask mechanisms in the process of ion beam etching.

In this Letter, we present a type of method of fabricating the tapered cavity layers of LVOFs based on ion beam etching with triangle-shaped mask and a normal film coating technique. The theory and structure design of the LVOF are introduced. We also propose the specific fabrication and measure process of a LVOF whose passband is 500–580 nm, and put more emphasis on discussing the experimental results.

A basic Fabry–Perot (FP) filter consists of two paralleled layers of metal mirrors and a center layer (resonant cavity) between them[16]. The passband wavelength of the filter can be tuned by varying the thickness of the resonant cavity. However, the transmission is restricted on account of the absorption of the metal. Thus, dielectric mirrors are utilized to replace the metal mirrors to promote the fundamental FP filter. The peak wavelength of the passband (λ_0) can be calculated according to the formula:

$$\lambda_0 = \frac{2nd}{k + (\varphi_1 + \varphi_2)/2} = \frac{2nd}{m}$$
$$m = k + (\varphi_1 + \varphi_2)/2, \qquad k = 0, 1, 2\ldots \tag{1}$$

where n and d are the refractive index and thickness of the center layer, and φ_1 and φ_2 are phases of the two reflected layers. It is indicated in this equation that the peak wavelength (λ_0) varies in direct proportion to the optical thickness (nd) of the center layer. Furthermore, provided that the thickness of the center layer is designed to be linearly tuned along the position in one direction, the linear variation of the peak wavelength of the passband can be obtained.

The pivot of the filter design is the choice of the materials for the layers. The difference between the two refractive index should be maximized, and conversely, the absorption of the material should be minimized. In this Letter, Ta_2O_5 and SiO_2 are selected as the high and low refractive materials, respectively. The practical index of the two materials for the needed spectral range are measured by an ellipsometer (UVISEL1, HORIBA JOBIN YVON, France) and shown in Fig. 1. In addition, the

 © 2015 Chinese Optics Letters

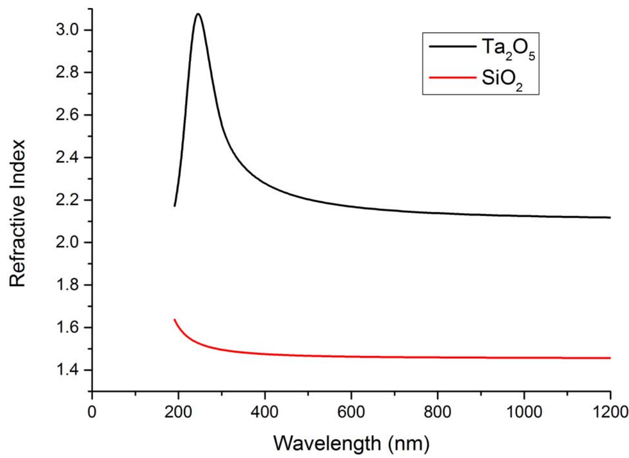

Fig. 1. Measured refractive indexes of Ta_2O_5 and SiO_2.

extinction coefficient of the both materials are deemed to be nearly zero for this wavelength range. Then, the measured data of the refractive indexes are imported to the thin film design software TFCalc. The multi-layered LVOF is designed for the 500–580 nm spectral range and the filter structure is as follows: Glass/ $H(LH)^5(x L)(HL)^5H$/Air, where L and H represent the low and high refractive index materials with an optical thickness of a quarter of the designed wavelength (550 nm), and x is the variation factor for the thickness of the cavity. $(HL)^5H$, xL, and $(HL)^5H$ stand for the thin film groups of the lower layer, the center layer, and the upper layer, respectively.

The transmission spectrum is calculated by using TFCalc, which is schematically depicted in Fig. 2. It can be noted that by increasing the thickness of the resonant cavity, the red shift of the peak wavelength is obtained, and the free spectral range (FSR) limits the passband wavelength. Apart from that, considering the higher spectral resolution and the broader FSR, the thickness of the cavity is set between 470 and 640 nm, and the peak wavelength is designed to be in the range of 500–580 nm. Meanwhile, on this premise, the average transmittance is about 75%, and the bandwidth and

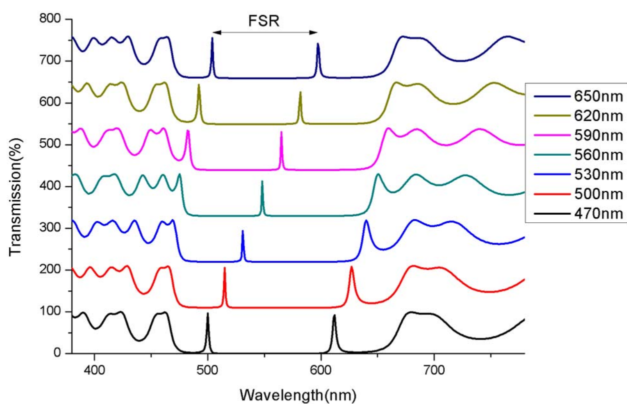

Fig. 2. Transmission spectra with different thicknesses of the resonant cavity.

the relative bandwidth are in the range of 1.5–2 nm and 0.27%–0.36%, respectively.

The wedge-shaped cavity is fabricated by fixing a mask between the ion source and the sample, and a designed triangle-shaped window has been opened in the center of the mask. During the ion beam etching, the sample is moved back and forth repeatedly at a constant velocity for the purpose of obtaining the linearly varied thickness of the cavity in the direction perpendicular to the shift orientation. The taper angle of the wedge can be accurately controlled by the number of times it is ion etched. The specific process flow is shown in Fig. 3. Firstly, the underneath and the center layer are deposited on the K9 substrate with an electron beam evaporation coating machine. After that, the wedge-shaped resonant cavity is fabricated using the method mentioned above. Finally, the upper layer is formed by coating the film similarly.

Figure 4 shows the schematic diagram of the ion beam etching for the wedge-shaped cavity with a reactive ion beam-etching machine (MRIBE-220M). The mask is a ceramic plate, which was fabricated in advance. The triangle-shaped window in the center can be designed arbitrarily according to the required wedge shape. The sample, the mask, and the ion source are set strictly parallel to each other. Moreover, the bottom margin of the triangle-shaped window and the undersurface of the sample are in one plane, and the height of the sample should be equal to the height of the triangle-shaped window.

It is shown in Fig. 5 that the length of the bottom margin and the height of the triangle are defined as L and H. The width of the window is set as D at different heights,

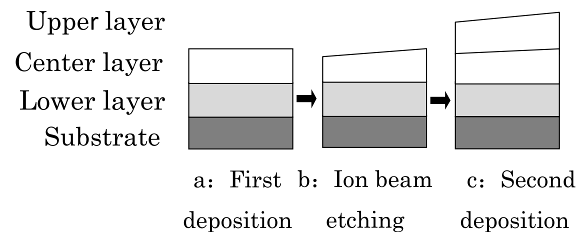

Fig. 3. Fabrication process flow of the designed LVOF.

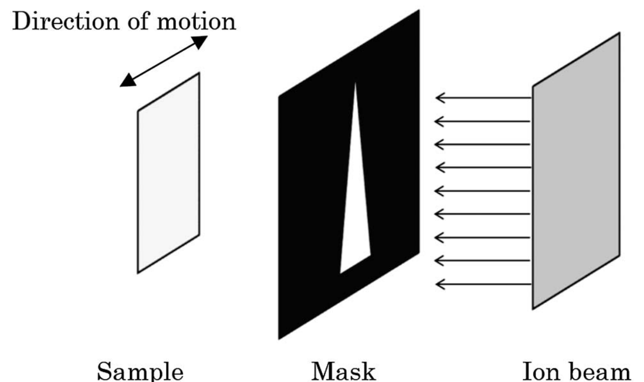

Fig. 4. Schematic diagram of ion beam etching.

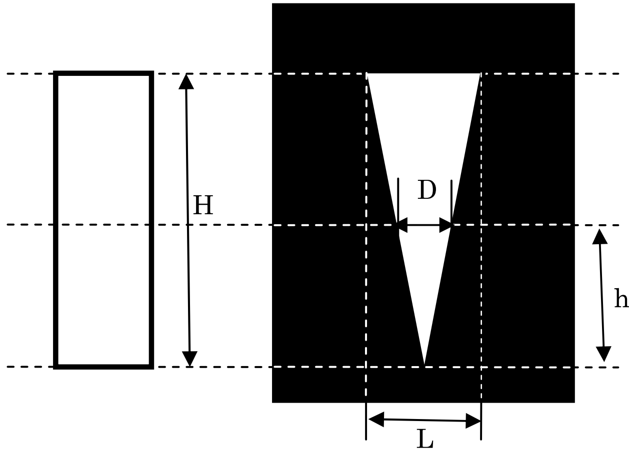

Fig. 5. Schematic diagram of sample and mask.

and the corresponding height is h. The function D of h can be expressed as the following equation:

$$D(h) = Lh/H. \tag{2}$$

The etching width (W) can be calculated as

$$W(h) = DvN/V = LhvN/(VH), \tag{3}$$

where v is the velocity of etching the center layer, V is the velocity of the shifted sample stage, and N is the number of etching times. The RF ion source we used is a rectangle that is 6 cm × 22 cm, and its inhomogeneity during etching can be controlled so that it is under 2%. In this Letter, the experiments adopt the same ion beam etching parameters: a beam voltage of 500 eV and a beam current of 200 mA. With the purpose of preparing for the ion beam etching, the standard velocity of etching SiO_2 is measured. Under the condition of Ar with 15 sccm and Ar/CF_4 with 5/10 sccm, the measured velocities of etching the SiO_2 are 1.33 and 3.83 nm/s. The number of etching times is calculated in accordance with the necessary etching depth and the etching efficiency of the material. The values of the surface roughness are 1.2 and 1.1 nm according to the results before and after ion beam etching measured by the atomic force microscope, respectively. We used the ellipsometer to investigate the variation of the thickness of the center layer. The measurement results show that the thickness of the center layer before the etching process is 652 nm, and after etching, the value changes to 455 nm at the thinner position of the wedge-shaped layer and 643 nm at the thicker position.

The transmission spectra of the fabricated device are measured by a spectrophotometer (Lambda 1050, HORIBA). Due to the linearly varied thickness of the LVOF, the size of the measuring light spot should be minimized. On the other hand, a spot that is too small would decrease the signal-to-noise ratio. Eventually, we put a tuned rectangle slit (0.6 mm) into the measure optical path and fixed it on a positioning system, as shown in Fig. 6. By adjusting the positioning system, the different positions of the LVOF can be measured.

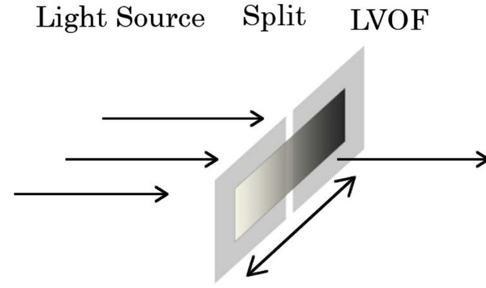

Fig. 6. Schematic diagram of sample and split.

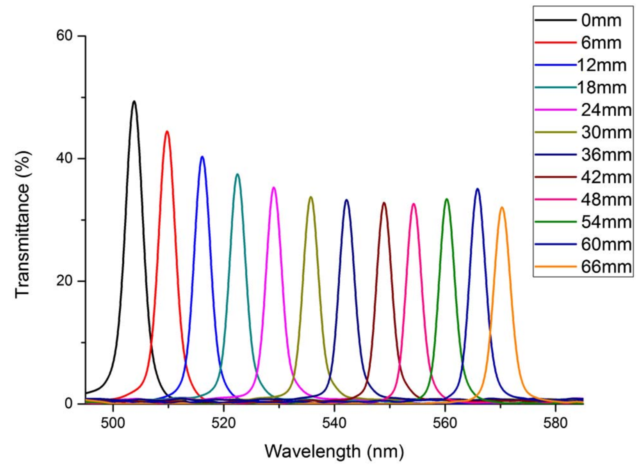

Fig. 7. Measured transmission spectra at different positions.

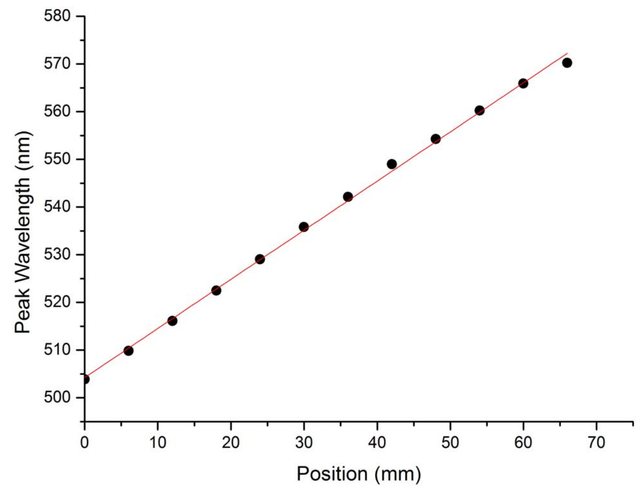

Fig. 8. Relationship between position and peak wavelength.

Figure 7 shows the experimental transmission of different positions on the device, where it can be seen that the transmission of the peak lies in 35%–52%, and the bandwidth is nearly 3 nm. It can be pointed out in Fig. 8 that there is a linear relationship between the peak wavelength

and the position, and their linearity can be up to 99.8%. Specifically, the linear dispersion is 1.03 nm/mm. To our knowledge, there are two reasons why the experimental transmission at peak wavelength is not high enough. One reason is that the designed transmitted bandwidth is very narrow, leading to sensitivity in the morphology of the center layer and the technological conditions. The surface roughness of the center layer and the optical asymmetry of the upper and lower layers would cause the decrease of the transmission and the broadening of the full-width at half maximum. The other reason is the width of the rectangular slit. The 0.6 mm length would cause the spectral shift of nearly 0.6 nm on the transmission spectra. As a result, the measured transmission is the average data of the many points in the range of the 0.6 mm length.

In conclusion, we present a method of fabricating the LVOF by fixing a designed mask between the ion source and sample. The resulting wedge-shaped cavity can be obtained by controlling the scanning frequency and time of ion beam etching. By using this method and combining it with coating technology, LVOFs whose transmission exceeds 40% for the wavelength of 500–580 nm are acquired. This method simply involves two procedures of coating the film and ion beam etching. This procedure has the advantages of a simplified process flow, tunable etching velocity, and arbitrary design over other fabrication methods. The taper angle of the wedge can be accurately controlled by controlling the number of times it is ion beam etched.

This work was partially supported by the National Natural Science Foundation of China (Nos. 61378060, 61205156, and 11105149) and the Innovation Program of the Shanghai Municipal Education Commission (No. 14YZ095).

REFERENCES

1. J. C. Demro, R. Hartshorne, and L. M. Woody, Proc. SPIE **2480**, 280 (1995).
2. L. Zhang, E. W. Anthon, J. C. Harrison, P. G. Hannan, F. J. Van Milligen, S. C. McEldowney, and S. Zarrabian, Proc. SPIE **3855**, 42 (1999).
3. A. Emadi, H. Wu, G. de Graaf, P. Enoksson, J. H. Correia, and R. Wolffenbuttel, Appl. Opt. **51**, 4308 (2012).
4. M. Ghaderi, N. P. Ayerden, A. Emadi, P. Enoksson, J. H. Correia, G. de Graaf, and R. F. Wolffenbuttel, J. Micromech. Microeng. **24**, 084001 (2014).
5. G. Minas, R. F. Wolffenbuttel, and J. H. Correia, J. Opt. A: Pure Appl. Opt. **8**, 272 (2006).
6. G. D. Caprio, D. Schaak, and E. Schonbrun, Biomed. Opt. Express **4**, 1486 (2013).
7. Y. Yu, X. Zhen, H. Zhang, and B. Zhou, Chin. Opt. Lett. **11**, 120601 (2013).
8. Z. Chen, J. Chen, Y. Li, J. Qian, J. Qi, J. Xu, and Q. Sun, Chin. Opt. Lett. **11**, 112401 (2013).
9. A. M. Piegari and V. Janicki, Proc. SPIE **5250**, 343 (2004).
10. R. R. McLeod and T. Honda, Opt. Lett. **30**, 2647 (2005).
11. L. Abel-Tibérini, F. Lemarquis, and M. Lequime, Appl. Opt. **47**, 5706 (2008).
12. A. Piegari and J. Bulir, Appl. Opt. **45**, 3768 (2006).
13. A. Piegari, J. Bulir, and A. K. Sytchkova, Appl. Opt. **47**, C151 (2008).
14. A. Emadi, H. Wu, S. Grabarnik, G. de Graaf, and R. F. Wolffenbuttel, J. Micromech. Microeng. **19**, 074014 (2009).
15. S. W. Wang, X. S. Chen, W. Lu, L. Wang, Y. Wu, and Z. S. Wang, Opt. Lett. **31**, 332 (2006).
16. H. A. Macleod, *Thin-Film Optical Filters* (CRC Press, 2001).